

# Spatial constraints underlying the retinal mosaics of two types of horizontal cells in cat and macaque

Stephen J. Eglen<sup>1,†</sup>, James C. T. Wong<sup>1</sup>

Revision: 1.26 August 7, 2012

<sup>1</sup> Cambridge Computational Biology Institute  
Department for Applied Mathematics and Theoretical Physics  
University of Cambridge  
Wilberforce Road, Cambridge CB3 0WA, UK

† Corresponding author.

Phone: +44 (0) 1223 765761

Email: S.J.Eglen@damtp.cam.ac.uk

Postprint of Visual Neuroscience (2008) 25:209–214. doi:10.1017/S0952523808080176

## Abstract

Most types of retinal neurons are spatially positioned in non-random patterns, termed retinal mosaics. Several developmental mechanisms are thought to be important in the formation of these mosaics. Most evidence to date suggests that homotypic constraints within a type of neuron are dominant, and that heterotypic interactions between different types of neuron are rare. In an analysis of macaque H1 and H2 horizontal cell mosaics, Wässle et al. (2000) suggested that the high regularity index of the combined H1 and H2 mosaic might be caused by heterotypic interactions during development. Here we use computer modelling to suggest that the high regularity index of the combined H1 and H2 mosaic is a by-product of the basic constraint that two neurons cannot occupy the same space. The spatial arrangement of type A and type B horizontal cells in cat retina also follow this same principle.

## Key words

horizontal cells, retinal mosaics, minimal distance model.

# Introduction

A defining feature for a type of retinal neuron is whether all neurons of that type tile the retina in non-random patterns, termed “retinal mosaics” (Cook, 1998). This definition can also help us, together with other anatomical and physiological properties, determine whether a group of neurons should be classified as one type, or subdivided into several types. For example, cat beta retinal ganglion cells (RGCs) are classed into two types, the on-centre beta RGCs and the off-centre beta RGCs, partly because the mosaic of either the on- or off-centre neurons independently tiles the retina and each mosaic is much more regular than the combined mosaic of all beta RGCs (Wässle et al., 1981). Furthermore, both cross-correlation analysis and modelling suggest that these two types of neuron are independent of each other in respect of positioning, as well as physiological function, and, hence, may develop independently (Wässle et al., 1981; Eglén et al., 2005). By contrast, Wässle et al. (2000) reported that for another pair of neuronal types, the H1 and H2 horizontal cells in macaque:

One would expect the nearest-neighbor distance of the combined mosaic to be smaller than that of the individual mosaics. The regularity index [defined in Methods, below], however, is comparable, suggesting that the H1 and H2 cells are not arrayed completely independently. It is possible, that some interaction between their mosaics during retinal development creates this overall regularity. (Wässle et al., 2000, p597)

In this report we use computer modelling to investigate whether the high regularity index of the combined mosaic of H1 and H2 neurons is a product of type-specific interactions between the two types, or whether it can be accounted for simply by anatomical constraints resulting from the two cell types occupying the same layer. To generalise this question slightly, and to evaluate more experimental data, we will compare the spatial patterning of horizontal cells in macaque with cat (Wässle et al., 1978).

## Methods

**Data sets** Three horizontal cell fields were analysed: fields A and B are from macaque (A: unpublished data; B: Figure 7 of Wässle et al. (2000)); field C is from cat (Figure 12 of Wässle et al. (1978)). To keep our notation concise (rather than claiming any equivalence of neuronal types across species), we denote type B cat horizontal cells as “type 1”, and type A horizontal cells as “type 2”, in line with previously-noted similarities of primate H1 and other mammalian B cells (de Lima et al., 2005). Fields were digitised, and the cell location taken to be the centre of each soma. Figure 1 shows an example real field along with a matching simulation, defined next.

**Bivariate  $d_{\min}$  model** We have generalised the  $d_{\min}$  model (Galli-Resta et al., 1997) to simulate the positioning of two neuronal populations within one field. Each type of neuron has its own homotypic exclusion zone ( $d_1$  or  $d_2$ ), but furthermore there is a heterotypic exclusion zone ( $d_{12}$ ) to potentially allow for exclusions between the two types of neuron. (The subscript  $_{12}$  refers to an interaction between two types of neuron, whereas the subscript  $_{1+2}$  used below refers to all neurons irrespective of type.) First, we count the number of type 1 and type 2 neurons ( $n_1$  and  $n_2$ ), and simulate an area  $A$  of the same size as the real field. To initialise the simulation, we randomly position  $n_1$  type 1 neurons and  $n_2$  type 2 neurons within  $A$ . Neurons are then repositioned randomly within the field subject to two constraints: that the nearest neighbour of the same type is greater than some distance ( $d_1$

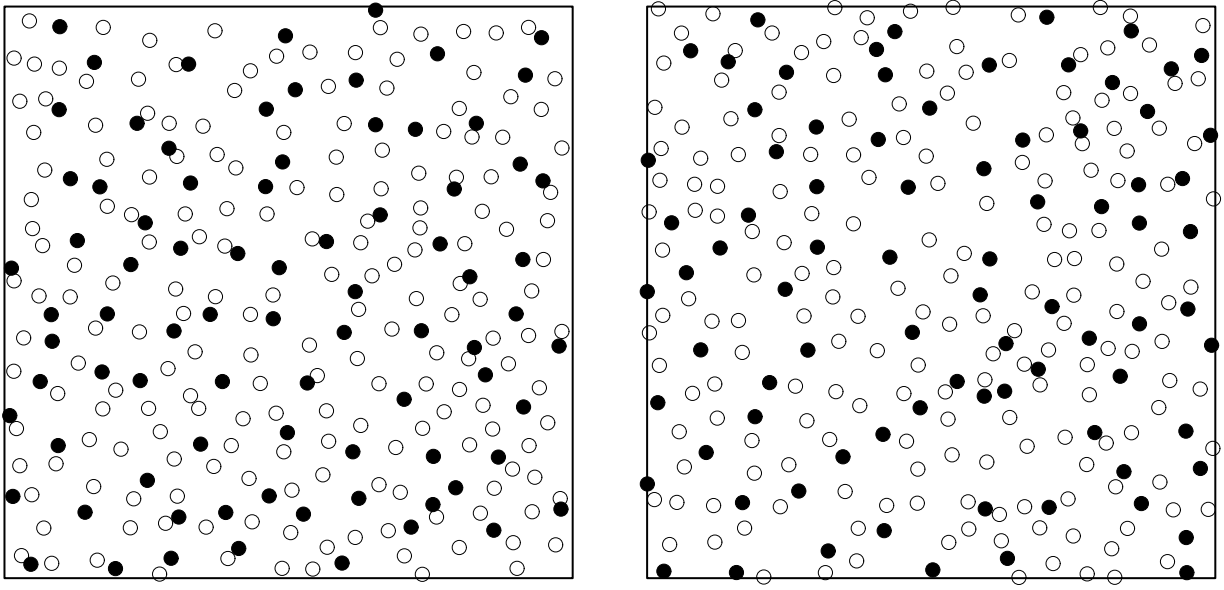


Figure 1: Real and simulated horizontal cell mosaics. Left: real mosaic (field A). Right: example simulation. Open circles denote H1 cells, filled circles denote H2 cells; cells drawn assuming  $10 \mu\text{m}$  diameter. Scale bar:  $100 \mu\text{m}$ . The simulated mosaic shows a close pair of H2 cells (halfway across, two-thirds up); such close pairs are rare but can occur when a homotypic exclusion zone is small.

for type 1 neurons,  $d_2$  for type 2 neurons), and that the nearest neighbour of the opposite type is greater than some distance  $d_{12}$ . Each of the distances  $d_1, d_2, d_{12}$  is a random variable drawn from a Normal distribution with a given mean and standard deviation. Random values lower than a lower limit ( $5 \mu\text{m}$ ) are discarded, to prevent implausibly small or negative  $d_{\min}$  values. This birth and death process (Ripley, 1977; Eglen et al., 2005) is repeated many times until convergence (typically after each neuron has been moved ten times).

**Null hypothesis** Somata of both types of horizontal cell occupy the same stratum of the inner nuclear layer (INL). (In this study, we ignore the small population of displaced horizontal cells that may be present in the ganglion cell layer (Silveira et al., 1989; Wässle et al., 2000).) Our null hypothesis states that the developmental interactions between the two types of neuron that influence their positioning are limited to preventing somal overlap: any two neurons, regardless of type, cannot come closer than some minimal distance. In the context of our simulations, this implies that the range of  $d_{12}$  should match the range of typical somal diameters of the two types of neuron.

**Parameter estimates** To fit one field, the free parameters in the model are the mean and standard deviation of the three exclusion zones. The homotypic exclusion zones ( $d_1, d_2$ ) were estimated first by fitting a univariate  $d_{\min}$  model (Galli-Resta et al., 1997) separately to the type 1 and type 2 neurons. The size of the heterotypic exclusion zone,  $d_{12}$ , was assumed to be of the same order as the soma diameter of the horizontal cells, around  $10 \mu\text{m}$ . Parameters were fitted by systematic searching over a range of plausible values.

**Assessing goodness of fit** Two measures were used to quantitatively compare our model against the real data, the regularity index (RI) and the K function. The RI is computed by

field	$n_1$	$n_2$	width $\times$ height ( $\mu\text{m}^2$ )	$d_1(\mu\text{m})$	$d_2(\mu\text{m})$	$d_{12}(\mu\text{m})$
A	187	82	400 $\times$ 402	22 $\pm$ 4	40 $\pm$ 10	11 $\pm$ 3.0
B	206	86	298 $\times$ 300	21 $\pm$ 4	32 $\pm$ 8	12 $\pm$ 2.5
C	300	85	723 $\times$ 1194	65 $\pm$ 12	72 $\pm$ 8	14 $\pm$ 3.0

Table 1: Parameters for each  $d_{\min}$  simulation. The number of type 1 and type 2 neurons ( $n_1$ ,  $n_2$ ) and the field size matches the values from the real field. The diameter of each exclusion zone ( $d_1$ ,  $d_2$ ,  $d_{12}$ ) is drawn from a Normal distribution, listed here as mean  $\pm$  standard deviation.

measuring the distance of each non-border neuron to its nearest-neighbour, and then dividing the mean of this distribution by its standard deviation (Wässle & Riemann, 1978). (Nearest-neighbour distances of neurons at the border of a field are excluded as those distances are unreliable. A neuron is excluded if its Voronoi polygon touches the boundary of the field. This exclusion criterion accounts for the small differences in RI between our work and those previously reported.) We measure three RI values:  $RI_1$  (distance of each type 1 neuron to nearest type 1 neuron),  $RI_2$ : (like  $RI_1$ , but for type 2 neurons), and  $RI_{1+2}$ : (distance of each neuron to nearest other neuron, irrespective of type).

For one population of neurons,  $K(t)$  measures the number of cell pairs within a given distance  $t$  of each other (Ripley, 1976; Eglen et al., 2005). For plotting purposes, we show  $L(t) = [K(t)/\pi]^{1/2}$ . This transformation discriminates between exclusion ( $L(t) < t$ ), clustering ( $L(t) > t$ ) and complete spatial randomness ( $L(t) = t$ ). We measure four L functions:  $L_1$ : pairs of type 1 neurons;  $L_2$ : pairs of type 2 neurons;  $L_{1+2}$ : pairs of neurons of either type. Finally,  $L_{12}$  measures the cross-correlation, by constraining cell pairs such that one cell is type 1 and the other is type 2. Full details of these measures are given elsewhere (Eglen et al., 2003, 2005).

To quantitatively evaluate the goodness of fit of the model to the real data, each simulation was run 99 times with the same parameters, but from different initial conditions. Informally, if the measure from the real data falls within the distribution of observed values from the simulations, then the model fits the data. This can be quantified with a p value using a Monte Carlo ranking test. A test statistic ( $T_i$ ) is measured for the K function of the real mosaic ( $i = 1$ ) and for each simulated mosaic ( $i = 2 \dots 100$ ). A p value is then calculated by dividing the rank (smallest first) of  $T_1$  by 100. P values greater than 0.95 indicate a significant difference at the 5% level between model and data. Full details of the test statistic are given in Eglen et al. (2005).

Computational modelling and analysis was performed in the R environment, using the `splancs` package and Voronoi domain software (R Development Core Team, 2007; Rowlingson & Diggle 1993; Fortune, 1987), as well as custom-written routines. The code is available from the authors upon request.

## Results and Discussion

Table 1 lists the parameters used for each bivariate  $d_{\min}$  simulation. The homotypic exclusion zones ( $d_1$ ,  $d_2$ ) were independently fitted to each mosaic, whereas the heterotypic exclusion zone ( $d_{12}$ ) was set to just prevent neurons of opposite type from occupying the same space in the inner nuclear layer. (Mean values of  $d_{12}$  reported in Table 1 are slightly higher than estimates of somal diameter, suggesting that both cell bodies and some initial portion of the primary dendrites contributed to steric hindrance between neuronal types.) Figure 2 shows that for each field, the model generates mosaics that quantitatively match the real mosaics, as assessed by both the RI and the L functions. In three (out of twelve) cases the

goodness of fit  $p$  value is greater than 0.95, indicating that formally there is a significant difference between data and model. Two of these cases concern both type 1 and type 2 neurons from cat retina (field C). Discrepancies in these two cases are apparent over small distances (less than  $10 \mu\text{m}$  between neurons of opposite type), and may be due simply to difficulties in reconstructing the position of pairs of opposite-type neurons that seem to overlap in the field from the original publication (Figure 12 of Wässle et al., 1978). Small errors in determining neuronal position are likely when considering the relative size of individual neurons with the size of the sample field. Overall, however, the L functions for the data fit within the confidence intervals of the model, suggesting that any disagreements between model and data are quite small.

Regularity of a  $d_{\min}$  mosaic is influenced by both neuronal density and the distribution of exclusion zone diameters. For both macaque fields, the median RI is higher for the simulated type 1 mosaics than for the simulated type 2 mosaics; the opposite is true for the cat field ( $p < 0.001$  in each of three cases, Wilcoxon rank sum test). The high RI of simulated cat type 2 mosaics, matching the observed data, is due to the relatively low s.d. in the type 2 exclusion zone (Table 1); if this is increased (e.g. from  $8 \mu\text{m}$  to  $16 \mu\text{m}$ ), the median  $RI_2$  decreases to 4.5 (data not shown), below that of the type 1 mosaics.

The RI of the combined type 1 and 2 mosaic ( $RI_{1+2}$ ) in each of our fields is typically 3–5, matching the values observed experimentally. At first glance, this might seem quite high, especially compared to a theoretical expected value of around 1.9 for cells (of infinitesimally small size) arranged randomly (Cook, 1996). Our model tells us that this high RI is simply a by-product of superimposing two regular, but independent, mosaics with somal exclusion. This conclusion can be supported in two ways. First, by setting  $d_{12}$  to zero, we eliminate all heterotypic interactions. (This allows for neurons of opposite type to become arbitrarily close to one another, which is of course not realistic, but allows us to specifically test the impact of removing all heterotypic interactions.) Figure 3A shows that  $RI_{1+2}$  drops considerably to a median of around 2.5, whereas the fits to  $RI_1$  and  $RI_2$  remain good. In this case, since there is no positional constraint between opposite-type neurons, the L function for the random simulations follows the theoretical expectation  $L_{12}(t) = t$ . The deviation between real data and simulations is apparent up to at least  $20 \mu\text{m}$  (Figure 3B), as observed by the L function for the real curve dropping well below the confidence intervals from the simulations.

The second line of evidence to explain the high RI of the combined (type 1 and type 2) mosaic is suggested by examining the fraction,  $f$ , of the retinal area occupied by the cell bodies. This can be estimated by  $f = ((n_1 + n_2)\pi r^2)/|A|$  where  $r = 5 \mu\text{m}$  is an estimate of radius of a horizontal cell soma,  $n_1$  and  $n_2$  are the number of type 1 and type 2 horizontal cells, and  $|A|$  is the area of the field. Table 2 shows that the fraction of occupancy ( $f$ ) correlates with the regularity of the combined mosaic ( $RI_{1+2}$ ). Furthermore, Table 2 also shows that the mean number of trial cell positions rejected due to infringement of the heterotypic constraint also correlates with the RI, even when normalised for the number of potential pairwise heterotypic interactions. In this light, the cat and macaque mosaics are generated by the same mechanism, and the lower regularity of the combined mosaic in cat is due to the smaller effect of somal exclusion.

Our bivariate  $d_{\min}$  model is open to criticisms of biological plausibility. As previously noted, exclusion models show us that local interactions are sufficient to generate regular patterns, but do not inform us on how these interactions are mediated (Galli-Resta et al., 1997). Here we would suggest that the homotypic exclusion zones are mediated by horizontal cell processes, perhaps driving lateral migration during development (Reese et al., 1999). The heterotypic interactions however are simply the result of steric hindrance between cell bodies and primary dendrites.

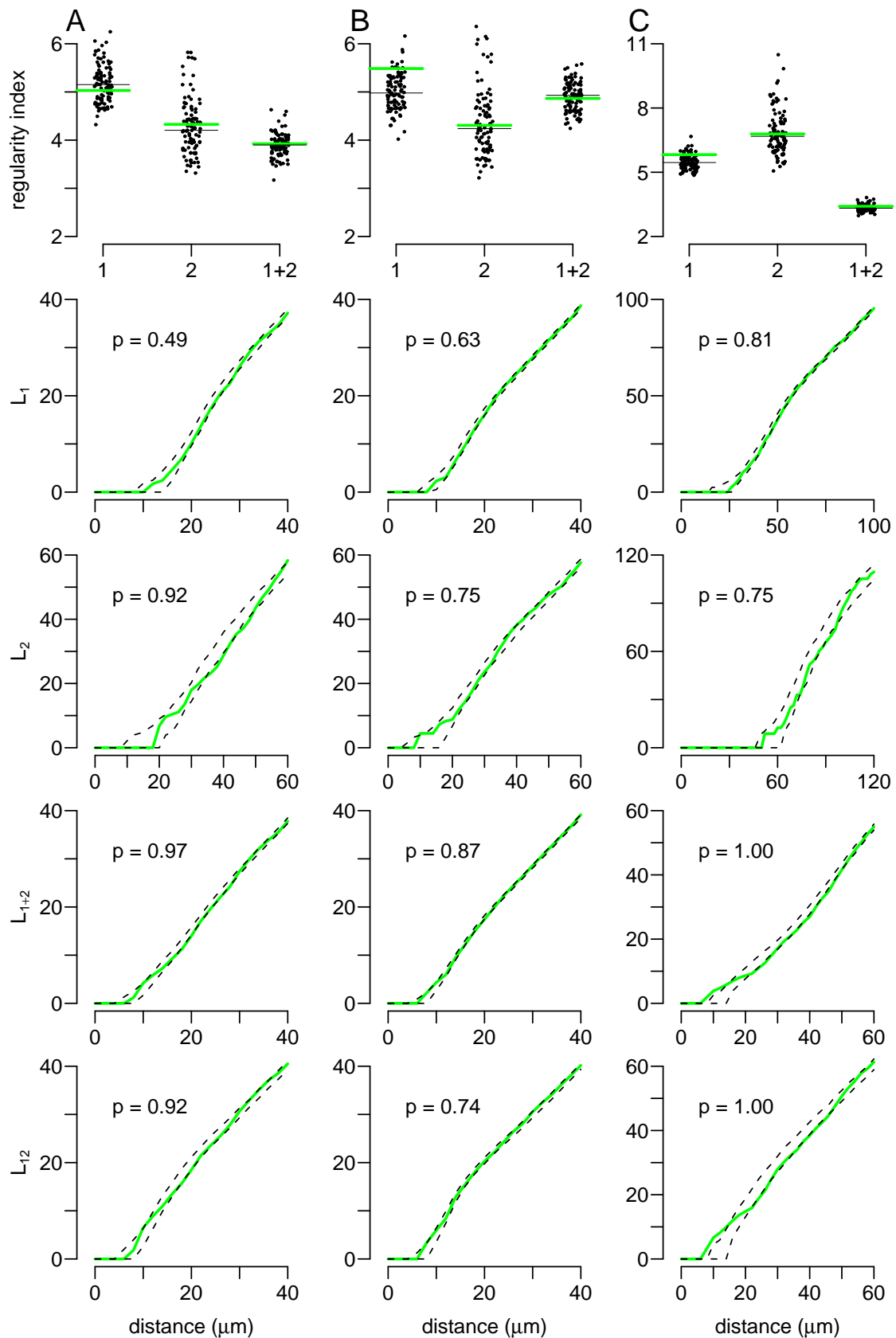


Figure 2: (Colour online.) Goodness of fit between data and model. Each column compares one field (A, B: macaque; C: cat) with simulations. In the regularity index (RI) plots, the thick green line indicates the RI of the real data for either type 1, type 2, or all (1+2) neurons. Black dots are RI values from 99 simulations, together with their median (thin black line). For each of four L function plots for a field, the L function for the real mosaic is shown as a solid green line and dashed black lines indicate 95% confidence intervals of simulations. The p value is the goodness of fit between model and data.

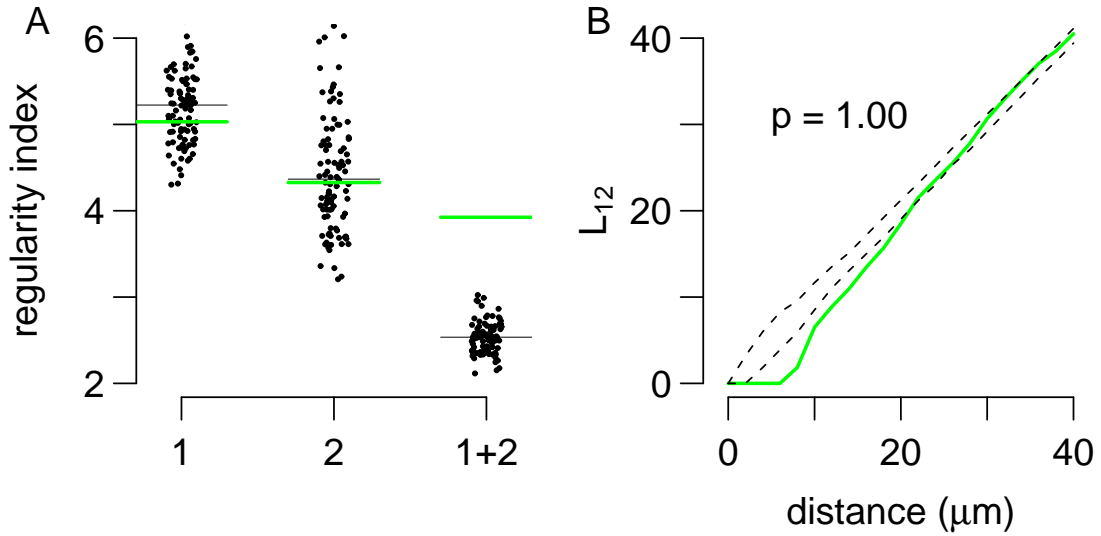


Figure 3: (Colour online.) Results of bivariate  $d_{\min}$  simulation for field A with  $d_{12} = 0$ , and other parameters as listed in Table 1. Results are presented as in Figure 2.

field	$RI_{1+2}$	$f$	rejects	$n_{\text{pairs}} = n_1 \times n_2$	rejects / $n_{\text{pairs}}$
C	3.4	0.04	$242 \pm 10$	25500	0.01
A	3.9	0.13	$940 \pm 32$	15334	0.06
B	4.9	0.26	$7198 \pm 282$	17716	0.41

Table 2: Estimates of the fraction  $f$  of sample retinal area occupied by all horizontal cell bodies in each field and incidence of heterotypic constraint enforcement. Rows are sorted in order of increasing regularity index of the combined mosaic. The mean ( $\pm$  s.d.) number of times (per sweep) that the heterotypic constraint was broken, rejects, was counted over 99 simulations. The final column shows the mean number of rejects divided by the number of pairs of opposite type neurons.

In conclusion, results from our computational model suggest that the high RIs observed for combined H1 and H2 mosaics in macaque are simply a by-product of the two mosaics being positioned in the same stratum of the INL; the mosaics may be developmentally independent in all other respects. This result agrees with our earlier work on beta RGCs (Eglen et al., 2005), as well as other studies demonstrating a lack of spatial correlations between many pairs of retinal neuronal types (Mack, 2007; Rockhill et al., 2000). Exceptions to this finding are rare (Kouyama & Marshak, 1997; Ahnelt et al., 2000).

**Acknowledgements** Thanks to Prof. Heinz Wässle for providing the unpublished field, labelled field A in this study, and to Prof. John Troy for critical reading of this manuscript. James Wong was supported by an EPSRC studentship.

## References

- Ahnelt, P. K., Fernández, E., Martinez, O., Bolea, J. A. & Kübber-Heiss, A. (2000). Irregular S-cone mosaics in felid retinas. Spatial interaction with axonless horizontal cells, revealed by cross correlation. *Journal of the Optical Society of America A* **17**, 580–588.
- Cook, J. E. (1996). Spatial properties of retinal mosaics: an empirical evaluation of some existing measures. *Visual Neuroscience* **13**, 15–30.
- Cook, J. E. (1998). Getting to grips with neuronal diversity. In Chaulpa, L. M. & Finlay, B. L., eds., *Development and organization of the retina*. Plenum Press, pages 91–120.
- de Lima, S. M. A., Ahnelt, P. K., Carvalho, T. O., Silveira, J. S., Rocha, F. A. F., Saito, C. A. & Silveira, L. C. L. (2005). Horizontal cells in the retina of a diurnal rodent, the agouti *Dasyprocta aguti*. *Visual Neuroscience* **22**, 707–720.
- Eglen, S. J., Raven, M. A., Tamrazian, E. & Reese, B. E. (2003). Dopaminergic amacrine cells in the inner nuclear layer and ganglion cell layer comprise a single functional retinal mosaic. *Journal of Comparative Neurology* **466**, 343–355.
- Eglen, S. J., Diggle, P. J. & Troy, J. B. (2005). Homotypic constraints dominate positioning of on- and off-centre beta retinal ganglion cells. *Visual Neuroscience* **22**, 859–871.
- Fortune, S. J. (1987). A sweepline algorithm for Voronoi diagrams. *Algorithmica* **2**, 153–172.
- Galli-Resta, L., Resta, G., Tan, S.-S. & Reese, B. E. (1997). Mosaics of Islet-1-expressing amacrine cells assembled by short-range cellular interactions. *Journal of Neuroscience* **17**, 7831–7838.
- Kouyama, N. & Marshak, D. W. (1997). The topographical relationship between two neuronal mosaics in the short wavelength-sensitive system of the primate retina. *Visual Neuroscience* **14**, 159–167.
- Mack, A. F. (2007). Evidence for a columnar organization of cones, Müller cells, and neurons in the retina of a cichlid fish. *Neuroscience* **144**, 1004–1014.
- R Development Core Team (2007). *R: A Language and Environment for Statistical Computing*. R Foundation for Statistical Computing, Vienna, Austria. ISBN 3-900051-07-0.
- Reese, B. E., Necessary, B. D., Tam, P. P. L., Faulkner-Jones, B. & Tan, S.-S. (1999). Clonal expansion and cell dispersion in the developing mouse retina. *European Journal of Neuroscience* **11**, 2965–2978.



- Ripley, B. D. (1976). The second-order analysis of stationary point processes. *Journal of Applied Probability* **13**, 255–266.
- Ripley, B. D. (1977). Modelling spatial patterns (with discussion). *Journal of the Royal Statistical Society B* **39**, 172–212.
- Rockhill, R. L., Euler, T. & Masland, R. H. (2000). Spatial order within but not between types of retinal neurons. *Proceedings of the National Academy of Sciences of the U.S.A.* **97**, 2303–2307.
- Rowlingson, B. S. & Diggle, P. J. (1993). Splancs: spatial point pattern analysis code in S-Plus. *Computers and Geosciences* **19**, 627–655.
- Silveira, L. C. L., Yamada, E. S. & Picanço-Diniz, C. W. (1989). Displaced horizontal cells and bplexiform horizontal cells in the mammalian retina. *Visual Neuroscience* **3**, 483–488.
- Wässle, H. & Riemann, H. J. (1978). The mosaic of nerve cells in the mammalian retina. *Proceedings of the Royal Society of London Series B* **200**, 441–461.
- Wässle, H., Peichl, L. & Boycott, B. B. (1978). Topography of horizontal cells in the retina of the domestic cat. *Proceedings of the Royal Society of London Series B* **203**, 269–291.
- Wässle, H., Boycott, B. B. & Illing, R. B. (1981). Morphology and mosaic of on-beta and off-beta cells in the cat retina and some functional considerations. *Proceedings of the Royal Society of London Series B* **212**, 177–195.
- Wässle, H., Dacey, D. M., Haun, T., Haverkamp, S., Grünert, U. & Boycott, B. B. (2000). The mosaic of horizontal cells in the macaque monkey retina: with a comment on bplexiform ganglion cells. *Visual Neuroscience* **17**, 591–608.